Experimental Two-Dimensional Infrared Spectra of Methyl Thiocyanate in Water and Organic Solvents

Joseph C. Shirley and Carlos R. Baiz

Department of Chemistry, University of Texas, Austin, TX, USA

Email: CRB, cbaiz@cm.utexas.edu

ABSTRACT

Thiocyanates, nitriles, and azides represent a versatile set of vibrational probes to measure structure and dynamics in biological systems. The probes are minimally perturbative, the nitrile stretching mode appears in an otherwise uncongested spectral region, and the spectra report on the local environment around the probe. Nitrile frequencies and lineshapes, however, are difficult to interpret, and theoretical models that connect local environments with vibrational frequencies are often necessary. However, the development of both more accurate and intuitive models remains a challenge for the community. The present work provides an experimentally consistent collection of experimental measurements, including IR absorption and ultrafast two-dimensional infrared (2D IR) spectra, to serve as a benchmark in the development of future models. Specifically, we catalog spectra of the nitrile stretching mode of methyl thiocyanate (MeSCN) in fourteen different solvents including non-polar, polar, and protic solvents. Absorption spectra indicate that π-interactions may be responsible for observed lineshape differences between aromatic and aliphatic alcohols. We also demonstrate that a recent Kamlet-Taft formulation describes the center frequency MeSCN. Further, we report cryogenic infrared spectra that may lead to insights into the peak asymmetry in aprotic solvents. 2D IR spectra measured in protic solvents serve to connect hydrogen bonding to static inhomogeneity. We expect that these insights, along with the publicly available dataset, will be useful to continue advancing future models capable of quantitatively describing the relation between local environments, lineshapes, and dynamics in nitrile probes.

I. INTRODUCTION

Vibrational spectroscopy is a powerful tool to study biological systems. The interpretation of peak positions and lineshapes can report on the structure of a species and the nature of its local environment. For example, amide I spectra are used to reveal *in vivo* protein secondary structure,[1] lipid ester carbonyls can report on hydration,[2–5] and phosphate modes can report on both lipids and nucleic acids.[6,7] These properties are important in biology, where the identity of chemical species is often known, and instead the configuration of molecules in a given system or process is of great interest. For example, consider biomolecular condensates, a topic of increasing study where much is still unknown about the localization of molecules and moieties, the transient secondary structures present, and the structure of water molecules within.[8,9] These new studies highlight that perhaps one of the most foundational properties of life is motion across many time and length scales from the picosecond fluctuations of hydrogen bonds to millisecond biological assembly formation.[10–12] Fortunately, time-resolved methods such as two-dimensional infrared (2D IR) spectroscopy have been developed to achieve the necessary time resolution to reach the fastest regimes.[13] In addition to time resolution, 2D IR also benefits from having two frequency axes, which spread out spectral information and reveal frequency fluctuations, interconversion, couplings, and energy exchange between different states.[13] Furthermore, 2D IR amplitudes scale with the fourth power of the transition dipole, which affords its narrower lineshapes and better background suppression when compared to linear techniques.[13] 2D IR has quickly gained traction due to these benefits, and a wide range of biological probes have been leveraged to provide new insights about the dynamics of lipid-water interfaces,[3–5,7] secondary structure couplings in proteins,[14] and the behavior of crowded systems.[15]

While intrinsic moieties are insightful and convenient probes, their ever-present nature provides some setbacks in terms of specificity *in vivo* or similarly congested environments.[16] The ester carbonyls of lipids, amide I modes of proteins, and ring modes of nucleic acids all appear in a similar spectral region, which is also heavily overlapped by the intense H-O-H bending modes of H_2O. In addition, a biological system may have countless lipids, sugars, nucleic acids, and proteins, each with its own spectral response. In the lab, sometimes these issues are avoided by isolating a system and making use of the shifted spectrum of D_2O, but understanding biological molecules in their native environments requires an inevitable return to the natural menagerie of biomolecules and, in some cases, H_2O.[17–19] Addressing the rising demand, vibrational probes such as azides, nitriles, and thiocyanates, which are rare or absent in natural systems and lie in a mostly unoccupied spectral window from 1800 cm^{-1} to 2500 cm^{-1}, have been developed.[20–27] Approaches to incorporate these probes into a host of biomolecules have been devised,[23] but proteins, in particular, have been the focus.[20] Thiocyanate, for example, can replace thiol groups on cysteine residues with post-translational chemical modifications. Likewise, nitriles can also be added to a variety of amino acids.[25] For direct incorporation of these probes, there are *in vivo* techniques such as amber codon suppression and *in vitro* techniques including solid-state peptide synthesis. On top of their expanding experimental accessibility and ideal spectral range, these probes also have other spectroscopic advantages, though weak oscillator strengths can be a limitation. This has been, however, recently addressed by the implementation of high repetition rate laser systems for 2D IR that further enhance signal-to-noise ratios.[28] Perhaps the most useful feature of these probes is the sensitivity of their spectral response to the local environment, which has been leveraged in Stark spectroscopy to investigate electric fields in proteins and other biomolecules.[29–34]

The sensitivity of azide, nitrile, and thiocyanate probes often becomes a limitation as the spectral changes in these probes can be incredibly complex to interpret. For probes such as ester carbonyls, some aspects of the lineshapes can correlate directly to a physical understanding of the system (e.g., a 15 cm^{-1} shift in frequency corresponds to the presence of a single hydrogen bond).[35] Yet thiocyanate (and its contemporaries) shows complex lineshape changes based on hydrogen bond angles, solvent exposure, and multiple electrostatic interactions.[36–38] In a well-defined system, these facets can be deconvolved given sufficiently detailed models to map specific interactions between probe and environment. However, *ad hoc* approaches often lack generalizability beyond the system of their genesis. Two studies on similar azide probes showed conflicting behavior of linewidths during a change in solvent exposure.[39,40] One additional challenge is the fact that measured spectral dynamics of these probes are convolved by the motions of the probe, the solvent, macromolecules, and almost anything else nearby.[24,41–43] To date, faithful reproductions of spectra and detailed interpretations of the behavior of these probes in any non-trivial environment have either relied on quantum mechanical simulations or other involved computational techniques. Quantum Mechanics / Molecular Mechanics (QM/MM) simulations implement quantum mechanical energy calculations into classical molecular dynamics, which allows for a more sophisticated determination of the energy of a vibrational probe.[43] Solvatochromism theory with Effective Fragment Potential (SolEFP) is a purpose-built molecular dynamics scheme that can more accurately describe complex vibrational probes by creating a trajectory of states where the frequency shifts related to a solute-solvent interaction potential that is partitioned into different components.[44–46] SolEFP has been designed with these azide, nitrile, and thiocyanate probes in mind, but does not reproduce peak asymmetry in aprotic solvents.[24]

There are two paths toward mending this issue. First, the more in-depth methods are continuing to grow in sophistication. Yet, there are still issues with the tractability of these calculations amongst the broader research community, especially in systems where computational efficiency is essential. As a second path, many theoretical and computational groups have been interested in creating robust, yet low-cost solutions for calculating infrared spectra of these probes in an expansive range of chemical environments. When considering the dynamic nature of these probes and the systems they inhabit, both ways forward require a comprehensive data set for benchmarking

the sub-picosecond dynamics of these probes. The purpose of the present work is to fill in the gap and create a reference point for further development in the field.

II. METHODS

A. FTIR Spectroscopy

MeSCN samples were prepared at 500 mM concentration in 12 organic solvents (acetone, acetonitrile [ACN], benzyl alcohol [BenzOH], *n*-butanol [n-ButOH], carbon tetrachloride [CCl_4], dimethyl sulfoxide [DMSO], ethanol [EtOH], ethyl acetate [EtAc], *n*-hexanol [n-HexOH], methanol [MeOH], *n*-propanol [n-PrOH], and tetrahydrofuran [THF]). They were prepared at 250 mM concentration in H_2O and 1 M in D_2O. The concentrations were determined by adding a fixed volume of solute to solvent and assuming linear addition of volume. For measurement, samples were pipetted between two CaF_2 windows with a 25 μm Teflon spacer. Spectra were recorded with 0.5 cm^{-1} resolution at room temperature (22 °C) using a Bruker INVENIO spectrometer.

For cryogenic measurements, samples were prepared similarly with a 25 μm spacer. Spectra were collected between 0 °C and -120 °C at 0.5 cm^{-1} resolution on a Bruker Vertex spectrometer using a Specac liquid-nitrogen cooled cryostat.

B. Two-Dimensional Infrared Spectroscopy

Ultrafast dynamics are measured using two-dimensional infrared (2D IR) spectroscopy. In brief, a pair of ultrafast (100 fs pulse width) excitation pulses cause $|0\rangle \rightarrow |1\rangle$ transitions within the sample. The system is allowed to propagate for a waiting time, t_2, and is then probed with a third pulse to generate and measure interactions between the $|0\rangle$ and $|1\rangle$ states and between the $|1\rangle$ and $|2\rangle$ states. The resulting spectrum correlates the excitation and detection frequency as a function of waiting time. The optical setup used is a pump-probe geometry which has been modified from the previously described optical setup,[47] and the measurement and data processing workflow has been described previously.[48] Here the spacing between pump pulse pairs was scanned between 0 fs and 4000 fs in steps of 20 fs using an acousto-optic modulator. An 1800 cm^{-1} rotating frame was used. The data was collected in a magic angle geometry to remove orientational effects. Waiting times were varied from 150 fs to 5000 fs. Each waiting time was collected with between 500,000 shots and 1,000,000 shots depending on the signal strength in each particular solvent. All 2D IR measurements were performed at room temperature (22 °C) with a sample cell identical to the one used in the FTIR measurements.

III. RESULTS AND DISCUSSION

A. Lineshapes and peak positions

If spectroscopy is to be used as a tool to take lineshapes and peak positions as input and determine the local environment around a probe, it is first necessary to do the reverse. Namely, the spectra of MeSCN must be collected and correlated with a well-understood set of local environments. This has been done both in an *ad hoc* manner and systematically for FTIR spectra several times before the present work, as described above. The systematic approach is continued and repeated here for two primary reasons. First, more insight into the lineshapes of the protic solvent has recently been described and can be added to the discussion of MeSCN spectra. Second, linear spectra represent an important baseline for the presentation and interpretation of multidimensional spectra. The solvent set has been selected to include commonly used organic solvents, such as DMSO, which has the furthest MeSCN redshift known of any organic solvent, and to demonstrate trends amongst protic solvents. FTIR spectra for each of the 14 solvents are summarized in **Figure 1** and their peak widths and positions are tabulated in **Table 1**.

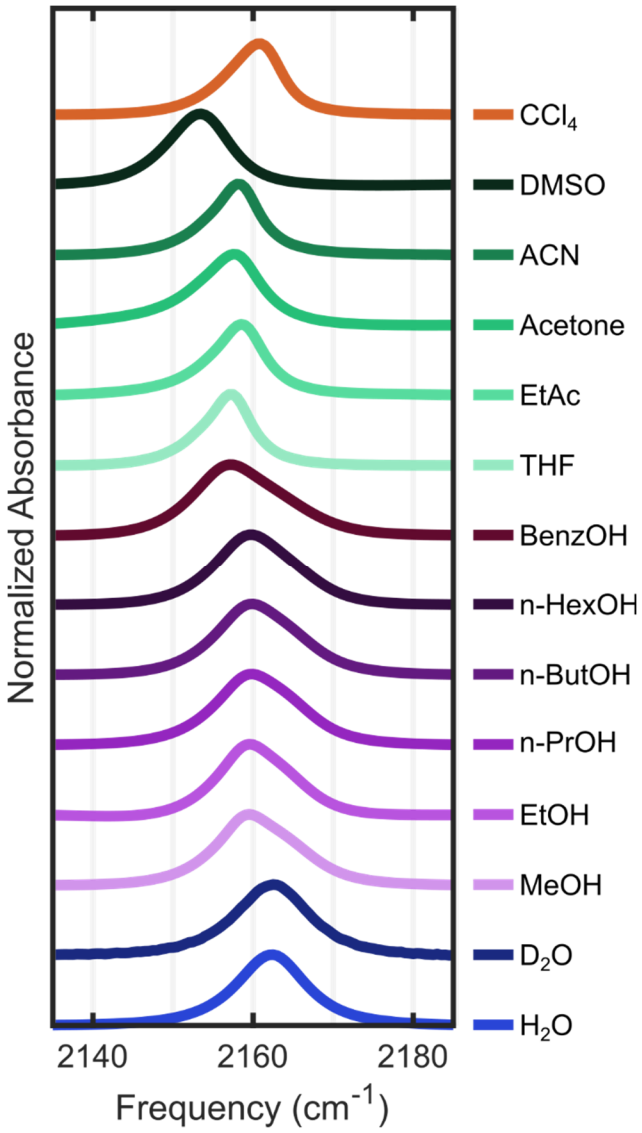

Figure 1 Measured absorption spectra of MeSCN in the CN stretching region for all the solvents reported here. Frequency in cm^{-1} is shown on the horizontal and normalized absorbance is on the vertical. Peaks are normalized by maximum. Water is shown in blue, alcohols in purple, other polar solvents in jade, and carbon tetrachloride in orange.

Table 1 First moment of the CN stretch and peak widths reported as the full width at half maximum (FWHM) are shown for MeSCN in each solvent. The first moment is determined by numerical integration of the peak area.

	First Moment (cm^{-1})	FWHM (cm^{-1})
CCl_4	2161.0	8.1
DMSO	2153.5	9.1
ACN	2158.0	7.4
Acetone	2157.5	9.4
EtAc	2158.5	7.8
THF	2157.0	7.1
BenzOH	2157.0	13.0
n-HexOH	2159.5	11.7
n-ButOH	2160.0	11.9
n-PrOH	2160.0	12.0
EtOH	2159.5	10.7
MeOH	2159.5	11.6
D_2O	2162.5	10.7
H_2O	2162.5	10.2

A considerable effort has been placed on understanding the underlying mechanism behind the lineshapes and frequencies for MeSCN. In water, computational studies have shown the symmetric lineshape is due to a balance between σ-type, π-type, and non-hydrogen-bonded species.[49] Similarly in aliphatic alcohols, the asymmetric shape is caused by σ-type hydrogen bonding in the higher energy region and unbonded MeSCN in the lower energy region.[36,49,50] MeSCN in benzyl alcohol is noticeably broader and the lower energy region is shifted further red when compared to its non-aromatic analogs. This could be due to interactions between the aromatic ring and the SCN moiety, as π-coupling should redshift the non-hydrogen-bonded region of the band. However, this phenomenon has not been explored in theoretical studies to our knowledge. In general, solvatochromic shifts can be related to the local electric field experienced by a vibrational probe via Onsager theory, which connects the electric field experienced by the solute to properties of the solvent, such as the dielectric and dipole moment, and properties of the solute, such as size.[42,44] For both the alcohols and water, theoretical work has shown that protic solvents are blueshifted from the center frequencies predicted by the Onsager field due to the electric field components added by the hydrogen bond donors, which are not appropriately described by the dielectric constant. Conversely, the central wavenumber in aprotic solvents is well correlated with the Onsager field due to the reduced complexity of their interactions. The central wavenumber and peak widths for thiocyanate have been more effectively described in the general case for both protic and aprotic solvents with SolEFP. SolEFP molecular dynamics methods produce a frequency fluctuation trajectory that can be used to generate infrared spectra. As mentioned before, peak asymmetry in aprotic solvents is one area where theoretical methods can still be improved. To provide a cursory investigation into the asymmetry for one solvent, spectra of MeSCN in THF have been collected under cryogenic conditions (**Figure 2**). Cryogenic conditions separate subpopulations by narrowing lineshapes, slowing the exchange of states, and reducing the populations of energetically unfavorable configurations. Peak asymmetry under these conditions can be enhanced or otherwise altered. Critically, the underlying geometry of subpopulations can change at low temperatures and these spectra should be supported by other techniques during further investigation.

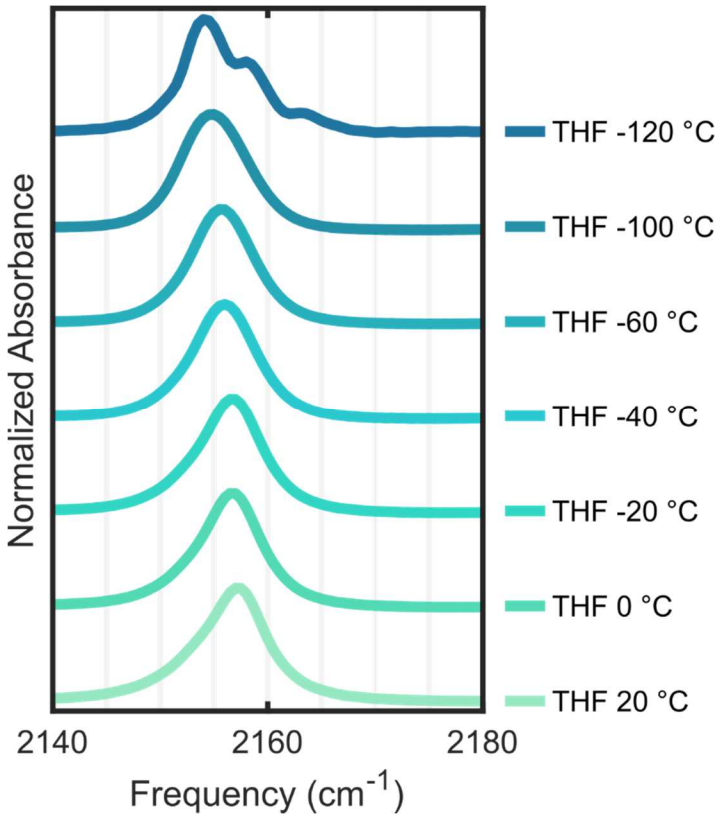

Figure 2 The CN stretching region of MeSCN in THF under cryogenic conditions. Frequency in cm^{-1} is shown on the horizontal axis and normalized absorbance is on the vertical axis. Peaks are normalized by maximum. The asymmetric peak becomes more symmetric while cooling and splits into multiple peaks after freezing. The freezing point of pure THF is -108.4 °C.

The temperature-dependent FTIR spectra show a noticeable change in peak asymmetry, position, and width over the range of temperatures. Notably, the peak shifts towards the red at lower temperatures. The freezing point of THF is -108.4 °C, and the frozen spectrum at -120 °C shows at least three distinct regions that contribute to the overall MeSCN lineshape in THF. Combined experimental and theoretical work has already found that thiocyanate ions in THF show multiple concentration-dependent peaks at room temperature and that these peaks are due to specific solute-solvent configurations.[51] Unlike ionic probes, MeSCN is not capable of forming ion pairs. Still, the asymmetric lineshapes in proteins at room temperature are known to be caused by distinct populations within the ensemble. This is similar to the asymmetric peaks of MeSCN in the protic solvents, which are due to specific hydrogen bonding configurations.[41,49] Therefore, it is likely that the asymmetry in MeSCN lineshapes in aprotic solvents is also due to distinct subpopulations. While many biochemical environments are protic, there are also numerous aprotic regions. As artificial vibrational probes continue to expand to regimes such as the lipid bilayer, hydrophobic protein cores, and beyond, future theoretical models will need to explain and reproduce the asymmetric lineshapes and their underlying mechanisms.

One traditional method of predicting solvatochromic shifts in peak position is to create an empirical interaction energy for solute-solvent interactions using the Kamlet-Taft parameters. Kamlet-Taft parameters are a set of empirical solvatochromic parameters that describe the hydrogen bond donating ability (α), hydrogen bond accepting ability (β), and polarizability (π*) of a solvent.[52] The MeSCN central frequencies have previously been fit with a linear combination of the Kamlet-Taft parameters, each parameter with its coefficient.[42,52] More recently, Gai and colleagues found that a significantly simpler combination of Kamlet-Taft parameters can predict the center frequency of cyanotryptophans, in this case, a single coefficient scaling the sum and difference of the coefficients (**Eq 1**).[53] $\delta\omega$ is the frequency shift and σ is the combined Kamlet-Taft parameter.

$$\delta\omega \propto \sigma \equiv \pi^* + \beta - \alpha \quad (1)$$

This simpler formulation can be extended to MeSCN as well (**Figure 3**). While empirical, the results show that the center frequency of the nitrile is directly correlated to a simple combination of solvent polarizability and hydrogen bond capabilities. A justification for this trend is that the π* parameter is generally linearly correlated to the dipole moment of a solvent, which itself is linearly correlated with the Onsager field. Therefore, the σ parameter is essentially a measure of the Onsager field with well-scaled solvatochromic hydrogen bonding corrections.

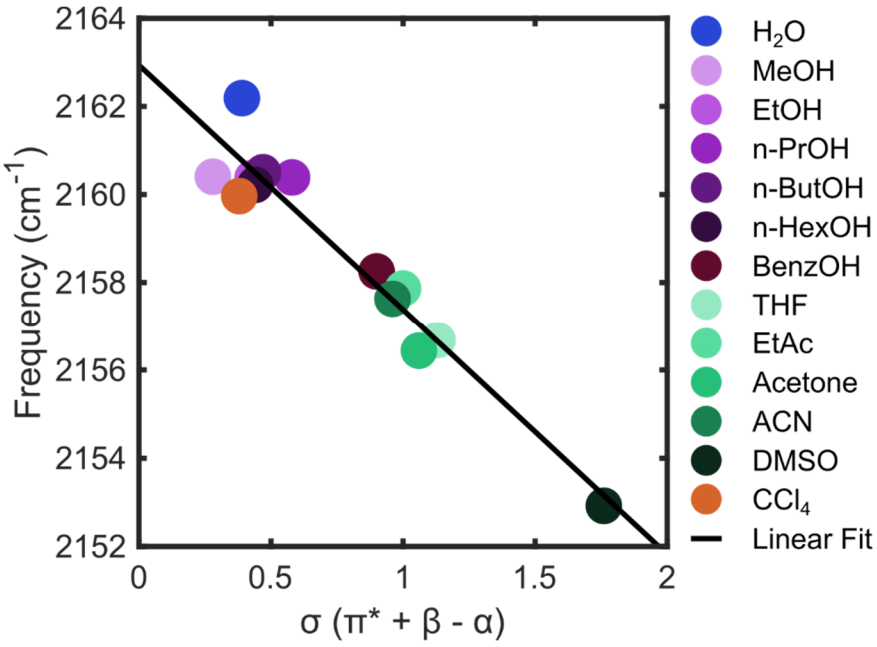

Figure 3 The MeSCN first moment plotted against σ, a combined Kamlet-Taft parameter which was originally correlated with 5-cyanotryptophan center frequency. Kamlet-Taft parameters are obtained from Marcus.[54] These data show a linear correlation with an R^2 value of 0.93.

The bulk of biochemically interesting environments are not well-behaved homogeneous solvents where the simplified treatment of the Onsager field (or its Kamlet-Taft derivative) applies, but this nevertheless demonstrates the prime importance of hydrogen bonding factors in any successful treatment of MeSCN frequencies.

B. Ultrafast Dynamics

As explained previously, lineshapes and peak positions are only part of the challenge for MeSCN predictive models. They are the more well-studied portion. Many of the spectroscopically relevant motions of the local solvent environment and of the probe itself occur on the timescale of femtoseconds to picoseconds. An in-depth interpretation of these dynamics in complex environments will require theoretical support, which in turn needs an experimental baseline. To gain information about these dynamics, 2D IR spectra were collected for MeSCN in each of the prior solvents. D_2O has been omitted from 2D IR measurements because of the overlap between the CN stretch and OD stretching modes. Three representative solvents and delays are shown in **Figure 4**. The complete set of plots is available in the Supporting Information. Measured FTIR and 2D IR spectra are available in the Texas Data Repository.[55]

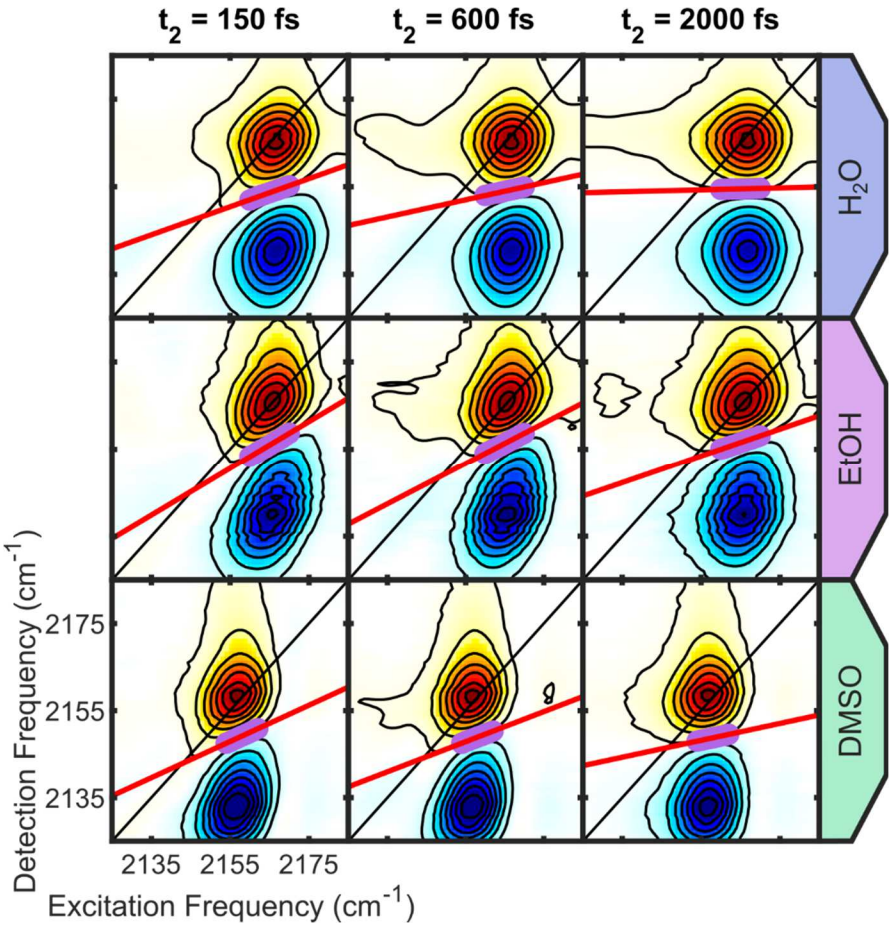

Figure 4 Select 2D IR from three solvents: H_2O, EtOH, and DMSO. The horizontal axis describes the pump (excitation) frequency, and the vertical describes the probe (detection) frequency, both in cm^{-1}. The correlation function is tracked by the nodal line, red, which is fit through the nodal points, light purple. t_2 is the waiting time, which varies by column.

Solvent dynamics were tracked using the nodal line slope (NLS). The nodal line slopes for each solvent were fit to a single exponential decay with a static offset. This functional form comes from Bloch dynamics where the frequency fluctuation correlation function (FFCF) is described by **Eq 2**. $C(t)$ is the FFCF, $\delta\omega$ is the frequency fluctuation, t_2 is the waiting time, T_2 is the homogeneous dephasing time, Δ_ω is the amplitude of the frequency fluctuations, τ is the correlation time in a single exponential decay, and Δ_0 is the static inhomogeneity.

$$C(t) = \langle \delta\omega(t_2)\delta\omega(0)\rangle = \frac{\delta(t_2)}{T_2} + \Delta_\omega^2 e^{\frac{-t_2}{\tau}} + \Delta_0^2 \quad \textbf{(2)}$$

The functional form of the NLS is given in **Eq 3**. In this form, a_0 becomes a unitless representation of the static inhomogeneity. Note that the inertial component related to the homogeneous dephasing time is left implicit.

$$NLS = a_\omega e^{\frac{-t_2}{\tau}} + a_0 \quad \textbf{(3)}$$

These correlation times and unitless static inhomogeneities are summarized in **Figure 5**. NLS decays are available in the Texas Data Repository.[55] The exponential fits are shown in **Figure S14**, and values are tabulated in **Table S1**.

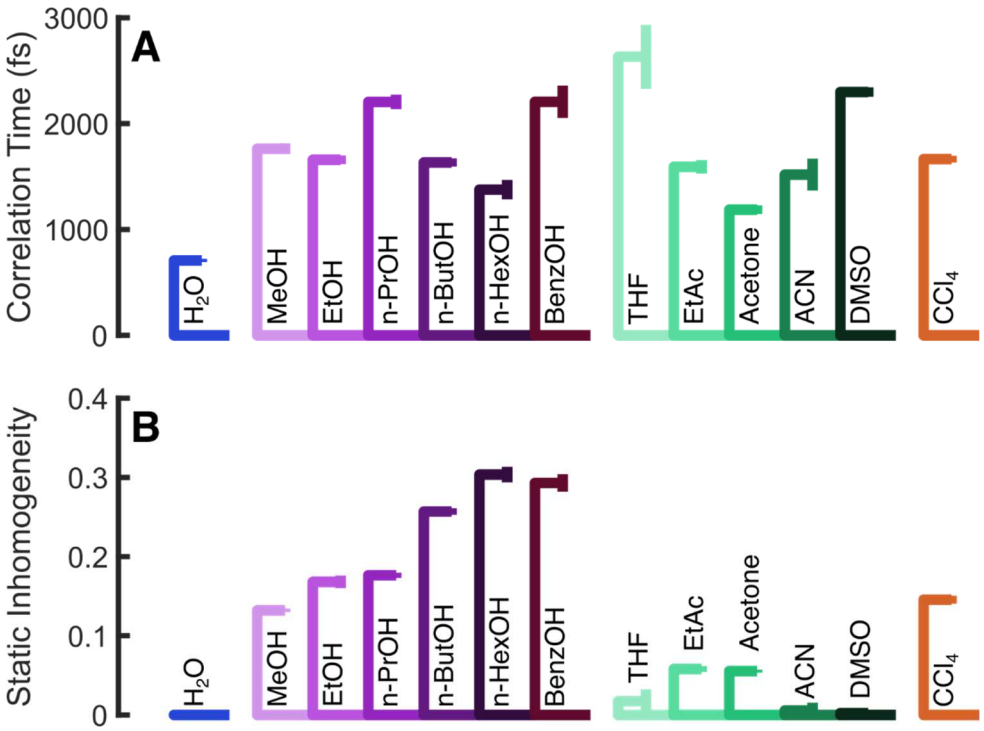

Figure 5 Correlation times (**A**) and static inhomogeneity values (**B**) extracted from exponential fits of the nodal line slope. Error bars are determined by bootstrapping the NLS fits and are shown as vertical lines. The exponential fits are shown in **Figure S14**, and values are tabulated in **Table S1**.

Given the timescale of the experiment was limited to 5 ps, the correlation times and static inhomogeneities can be interpreted as follows. Spectral diffusion less than 5 ps is typically related to the motions of the solvent and solute within the first solvation shell. The static inhomogeneous component is essential a sum of all processes that occur beyond the 5 ps cutoff, which can include diffusive motions or macromolecular behavior when applicable. Given these interpretations, there are several trends in the data from **Figure 5**. Focusing on the correlation times of protic solvents first, the frequency fluctuations in H_2O are notably faster than any other solvent. Prior 2D IR studies have found similar measurements of correlation time and inhomogeneity of MeSCN in water.[23,56,57] These experimental studies, along with theoretical works, relate the dynamics of MeSCN in H_2O to hydrogen bond fluctuations and local reorganization.[58] Water causes these fast fluctuations because both its hydrogen-bond-donating sites and lone pairs are in motion and shift MeSCN vibrational energies. Furthermore, the networked nature of water hydrogen bonds allows for fast structural rearrangements because the energetic cost of breaking hydrogen bonds is readily paid for by the formation of new bonds.[10] In contrast, methanol has half of the donatable hydrogens of water, is about twice the size, does not have the same extended network, and, consequently, has about twice the correlation time. However, the relative size may not be quite as important because it does not hold for aliphatic alcohols in general, with hexanol having the fastest spectral diffusion and no particular trend amongst the series. Prior studies have indicated that only one alcohol molecule is in a hydrogen bond configuration with MeSCN at a given time.[50] Together, these facts indicate that the dynamic frequency fluctuations experienced by the MeSCN are not due to more extended solvent rearrangements in the alcohols. Indeed, the restructuring motions of alcohols manifest in the static inhomogeneity, increasing with the size of the alcohol. In other words, the dynamics experienced by MeSCN on the 5 ps timescale are generally not related to large protic solvent motions, but the relative proportion of quasi-static processes increases as the solvent rearrangement time increases. There is a linear correlation between the inhomogeneity and the tail length/mass/viscosity of the aliphatic alcohols (R^2 = 0.94/0.94/0.92) (**Figure S15**). Prior work has suggested that slower components of spectral diffusion in localized vibrational modes can be related to viscosity due to a diffusive movement of solvent molecules in the solvation shell of the probe.[59] The similar trend in slowing has been observed with a delocalized probe in aliphatic alcohols but did not match the timescale of

diffusion due to the delocalization.[60,61] These slower components of spectral diffusion can translate into static inhomogeneity when the timescale of the experiment and responsiveness of the probe change.

There is also a trend that, in general, the aprotic solvents have significantly lower static inhomogeneity than the protic solvents, sometimes approaching zero. This indicates that most frequency-modulating changes in the local solvent environment occur on a timescale faster than 5 ps for these solvents. These aprotic solvents also tend to have narrower linewidths than the protic solvents. Linewidth in methyl thiocyanate has previously been associated with faster solvent motions.[41] However, there is no relationship in the present work between the NLS correlation times and the FWHM (R^2 = 0.00) (**Figure S16**). Instead, there is a correlation between the FWHM and the amplitude of the inertial component of the NLS decay, which is the difference between 1 and the fit amplitude of the exponential decay and static component of the NLS (**Figure 6**). For a single peak, this term is related to the reciprocal homogeneous dephasing time (**Eq 2**). When the inertial amplitude is larger, the resulting spectra are more homogeneous and can experience motional narrowing. The associated 2D spectra of the aprotic solvents are rounder at short waiting times than the alcohols (**Figures S1 to S13**). One caveat is that part of the linewidth in the protic solvents is due to specific hydrogen bonding ensembles, rather than a simple lack of homogeneity. Nonetheless, these findings imply that some solvent motions contributing to linewidth may be faster than the current time resolution accessible by 2D IR spectroscopy.

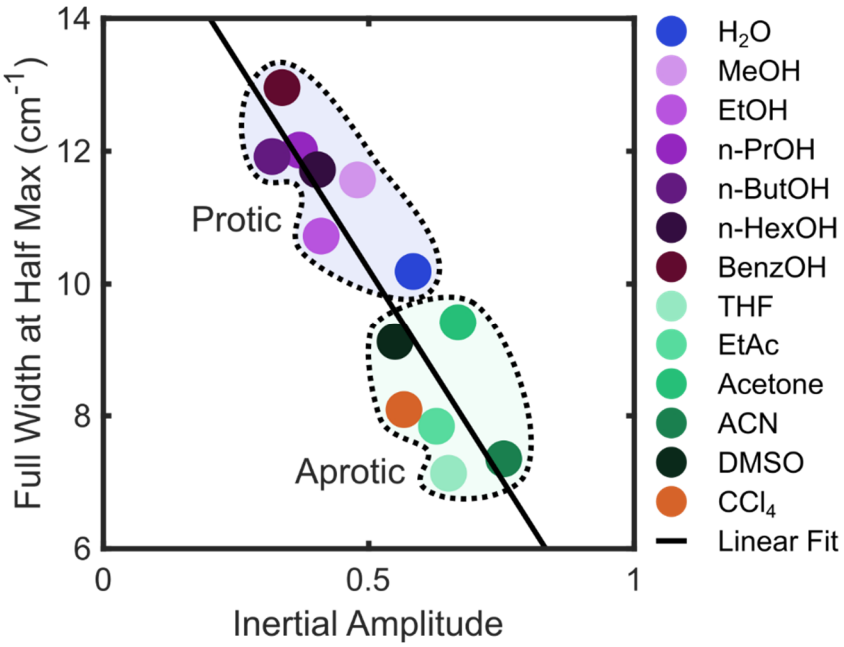

Figure 6 Correlation between the inertial component of the NLS (horizontal axis) and the FTIR FWHM (vertical axis). The inertial component is the difference between 1 and the fit amplitude of the exponential decay and static component of the NLS. These are fluctuations that occur faster than the timescale of the 2D IR experiment. R^2 = 0.80.

In contrast to the inhomogeneous component, the variations in spectral diffusion among the aprotic solvents are not easily explained. In the literature, there are varied examples of spectral diffusion for thiocyanates at these waiting times. One work compared thiocyanate-labeled sugars in water and chloroform and showed that the samples in chloroform had an extra spectral diffusion process on the order of 5 to 6 ps.[23] For a thiocyanate probe on hemoglobin, it was found that some spectral diffusion occurs on a timescale of less than 5 ps, which was attributed to dynamic rearrangements and interactions with the environment, but no specific correlation time could be extracted.[42] The same work attributed other correlation times of MeSCN in different aprotic solvents simply to solvent motions. The trend between these two works is that the dynamic processes of aprotic solvents and their interplay with nitrile peaks remain mysterious.

In summary, hydrogen bonding capabilities of the local environment play a large role in the spectral behavior of MeSCN. In purely aqueous conditions, the dynamics are fast, and a complete loss of correlation occurs before 5 ps. However, when there are slower solvent processes, the vibrational energy of some microstates remains unchanged even after long waiting times. In the absence of hydrogen bond donors, long-time correlations are rarer but highly solvent-dependent.

IV. SUMMARY AND CONCLUSION

Researchers working with biochemical systems have a strong interest in transparent-window vibrational probes. Thiocyanate has many features that make it desirable, including sensitivity, a long vibrational lifetime, and chemistries for installation at a wide variety of sites. Because of its importance, there is a continued push for more in-depth and more accessible models. Initially, the Skinner group[62–64] developed a reparameterization technique (followed by Corcelli and colleagues)[65,66] to compute azide and nitrile frequencies with optimized quantum mechanics/molecular mechanics (OQM/MM). Around the same time, theoretical work on the system by Cho and coworkers focused on understanding spectral shifts due to hydrogen bonding and the parameterization of an electrostatic vibrational map.[36,37,50] The OQM/MM techniques need to be reparametrized when moving too far away from the calibration system, and it has been shown that electrostatic vibrational maps are also not easily expanded to more than one chemical environment.[49] Consequently, the OQM/MM methods have been used in some protein systems[67,68], and the QM framework underlying the vibrational maps has been expanded and used to deconvolve frequency fluctuations based on the interacting species.[43] While powerful, further development of generalizable vibrational models must include more in-depth calculations across a wider range of systems that capture not only electrostatic environments but also dynamics. New approaches such as stochastic models that take advantage of frequency-dependent friction effects may provide an alternative approach to modeling spectra of nitriles.[69] The results here show that dynamics are key to both reproducing accurate lineshapes and understanding molecular processes. One additional caveat is that protein environments are not like solvents; they are far removed from simple dielectrics, and each site presents a unique environment with its dynamic processes. In addition to these properties, limitations in the soluble concentrations and the sheer size make systematic studies into protein-bound vibrational probes a significant hurdle for both experimentalists and theorists.

Whether to expand computationally efficient models or to compare the state of the art, to our knowledge, time-dependent infrared spectra of MeSCN in a broad range of solvents have not been made publicly available. To this end, the present work provides an experimental basis for the development of theory with a high-quality, publicly available set of data.[55] It also provides insight into the dynamics of methyl thiocyanate, such as evidence that diffusive solvent motions drive static inhomogeneity measurements on the picosecond timescale and that hydrogen bonding is a large contributor to inhomogeneity. Furthermore, cryogenic FTIR measurements hint at an area of further study for understanding the lineshapes of MeSCN. Thiocyanates are both scientifically valuable and complex, and the continued development of spectroscopic theory is perhaps one of the current factors limiting the insight we can gain from experiments. While simple solvent systems are a starting point, systemic approaches to proteins and other biomolecules will be needed in the future. Advancing theoretical models is central to further development and applications of these vibrational probes and spectroscopy in general.

Data Availability Statement: The data that support the findings of this study are openly available in the Texas Data Repository at https://doi.org/10.18738/T8/JLUVIR

Acknowledgments: We thank Ziareena A. Al-Mualem for acquiring some of the FTIR and 2D IR data. We also thank the financial support of the National Science Foundation (CHE-1847199) and the Welch Foundation (F-1891). We thank the Texas Advanced Computing Center for the computing resources used in this work.

v. REFERENCES

(1) Baiz, C. R.; Reppert, M.; Tokmakoff, A. An Introduction to Protein 2D IR Spectroscopy. In *Ultrafast Infrared Vibrational Spectroscopy*; Fayer, M. D., Ed.; Taylor & Francis: New York, 2013; pp 361–403. https://doi.org/10.1201/b13972.

(2) You, X.; Lee, E.; Xu, C.; Baiz, C. R. Molecular Mechanism of Cell Membrane Protection by Sugars: A Study of Interfacial H-Bond Networks. *J. Phys. Chem. Lett.* **2021**. https://doi.org/10.1021/acs.jpclett.1c02451.

(3) Valentine, M. L.; Waterland, M. K.; Fathizadeh, A.; Elber, R.; Baiz, C. R. Interfacial Dynamics in Lipid Membranes: The Effects of Headgroup Structures. *J. Phys. Chem. B* **2021**, *125* (5), 1343–1350. https://doi.org/10.1021/acs.jpcb.0c08755.

(4) Flanagan, J. C.; Valentine, M. L.; Baiz, C. R. Ultrafast Dynamics at Lipid–Water Interfaces. *Acc. Chem. Res.* **2020**, *53* (9), 1860–1868. https://doi.org/10.1021/acs.accounts.0c00302.

(5) Flanagan, J. C.; Cardenas, A. E.; Baiz, C. R. Ultrafast Spectroscopy of Lipid–Water Interfaces: Transmembrane Crowding Drives H-Bond Dynamics. *J. Phys. Chem. Lett.* **2020**, *11* (10), 4093–4098. https://doi.org/10.1021/acs.jpclett.0c00783.

(6) Schauss, J.; Kundu, A.; Fingerhut, B. P.; Elsaesser, T. Contact Ion Pairs of Phosphate Groups in Water: Two-Dimensional Infrared Spectroscopy of Dimethyl Phosphate and Ab Initio Simulations. *J. Phys. Chem. Lett.* **2019**, *10* (20), 6281–6286. https://doi.org/10.1021/acs.jpclett.9b02157.

(7) Costard, R.; Heisler, I. A.; Elsaesser, T. Structural Dynamics of Hydrated Phospholipid Surfaces Probed by Ultrafast 2D Spectroscopy of Phosphate Vibrations. *J. Phys. Chem. Lett.* **2014**, *5* (3), 506–511. https://doi.org/10.1021/jz402493b.

(8) N. Edun, D.; R. Flanagan, M.; L. Serrano, A. Does Liquid–Liquid Phase Separation Drive Peptide Folding? *Chem. Sci.* **2021**, *12* (7), 2474–2479. https://doi.org/10.1039/D0SC04993J.

(9) Lorenz-Ochoa, K.; Baiz, C. Ultrafast Spectroscopy Reveals Slow Water Dynamics in Biocondensates. ChemRxiv August 10, 2023. https://doi.org/10.26434/chemrxiv-2023-6ml88.

(10) Laage, D.; Hynes, J. T. A Molecular Jump Mechanism of Water Reorientation. *Science* **2006**, *311* (5762), 832–835. https://doi.org/10.1126/science.1122154.

(11) Shin, S.; Willard, A. P. Quantifying the Molecular Polarization Response of Liquid Water Interfaces at Heterogeneously Charged Surfaces. *J. Chem. Theory Comput.* **2023**, *19* (6), 1843–1852. https://doi.org/10.1021/acs.jctc.2c01256.

(12) Ebbinghaus, S.; Kim, S. J.; Heyden, M.; Yu, X.; Heugen, U.; Gruebele, M.; Leitner, D. M.; Havenith, M. An Extended Dynamical Hydration Shell around Proteins. *Proc. Natl. Acad. Sci.* **2007**, *104* (52), 20749–20752. https://doi.org/10.1073/pnas.0709207104.

(13) Hamm, P.; Zanni, M. *Concepts and Methods of 2D Infrared Spectroscopy*; Cambridge University Press: New York, 2011; Vol. 9781107000. https://doi.org/10.1017/CBO9780511675935.

(14) Smith, A. W.; Chung, H. S.; Ganim, Z.; Tokmakoff, A. Residual Native Structure in a Thermally Denatured β-Hairpin. *J. Phys. Chem. B* **2005**, *109* (36), 17025–17027. https://doi.org/10.1021/JP053949M/ASSET/IMAGES/LARGE/JP053949MF00002.JPEG.

(15) You, X.; Shirley, J. C.; Lee, E.; Baiz, C. R. Short- and Long-Range Crowding Effects on Water's Hydrogen Bond Networks. *Cell Rep. Phys. Sci.* **2021**, *2* (5), 100419. https://doi.org/10.1016/j.xcrp.2021.100419.

(16) Tros, M.; Zheng, L.; Hunger, J.; Bonn, M.; Bonn, D.; Smits, G. J.; Woutersen, S. Picosecond Orientational Dynamics of Water in Living Cells. *Nat. Commun.* **2017**, *8* (1), 904. https://doi.org/10.1038/s41467-017-00858-0.

(17) Ellis, R. J.; Minton, A. P. Join the Crowd. *Nature* **2003**, *425* (6953), 27–28. https://doi.org/10.1038/425027a.

(18) Yeon Chun, S.; Kook Son, M.; Ri Park, C.; Lim, C.; I. Kim, H.; Kwak, K.; Cho, M. Direct Observation of Protein Structural Transitions through Entire Amyloid Aggregation Processes in Water Using 2D-IR Spectroscopy. *Chem. Sci.* **2022**, *13* (16), 4482–4489. https://doi.org/10.1039/D1SC06047C.

(19) Giubertoni, G.; Bonn, M.; Woutersen, S. D2O as an Imperfect Replacement for H2O: Problem or Opportunity for Protein Research? *J. Phys. Chem. B* **2023**, *127* (38), 8086–8094. https://doi.org/10.1021/acs.jpcb.3c04385.

(20) Lindquist, B. A.; Furse, K. E.; Corcelli, S. A. Nitrile Groups as Vibrational Probes of Biomolecular Structure and Dynamics: An Overview. *Phys. Chem. Chem. Phys.* **2009**, *11* (37), 8119–8132. https://doi.org/10.1039/B908588B.

(21) Fafarman, A. T.; Webb, L. J.; Chuang, J. I.; Boxer, S. G. Site-Specific Conversion of Cysteine Thiols into Thiocyanate Creates an IR Probe for Electric Fields in Proteins. *J. Am. Chem. Soc.* **2006**, *128* (41), 13356–13357. https://doi.org/10.1021/ja0650403.

(22) Ma, J.; Pazos, I. M.; Zhang, W.; Culik, R. M.; Gai, F. Site-Specific Infrared Probes of Proteins. *Annu. Rev. Phys. Chem.* **2015**, *66*, 357–377. https://doi.org/10.1146/annurev-physchem-040214-121802.

(23) Gasse, P.; Stensitzki, T.; Mai-Linde, Y.; Linker, T.; Müller-Werkmeister, H. M. 2D-IR Spectroscopy of Carbohydrates: Characterization of Thiocyanate-Labeled β-Glucose in CHCl3 and H2O. *J. Chem. Phys.* **2023**, *158* (14), 145101. https://doi.org/10.1063/5.0139166.

(24) Błasiak, B.; Londergan, C. H.; Webb, L. J.; Cho, M. Vibrational Probes: From Small Molecule Solvatochromism Theory and Experiments to Applications in Complex Systems. *Acc. Chem. Res.* **2017**, *50* (4), 968–976. https://doi.org/10.1021/acs.accounts.7b00002.

(25) Adhikary, R.; Zimmermann, J.; Romesberg, F. E. Transparent Window Vibrational Probes for the Characterization of Proteins With High Structural and Temporal Resolution. *Chem. Rev.* **2017**, *117* (3), 1927–1969. https://doi.org/10.1021/acs.chemrev.6b00625.

(26) Thielges, M. C. Transparent Window 2D IR Spectroscopy of Proteins. *J. Chem. Phys.* **2021**, *155* (4), 040903. https://doi.org/10.1063/5.0052628.

(27) Salehi, S. M.; Meuwly, M. Site-Selective Dynamics of Ligand-Free and Ligand-Bound Azidolysozyme. *J. Chem. Phys.* **2022**, *156* (10), 105105. https://doi.org/10.1063/5.0077361.

(28) Donaldson, P. M.; Greetham, G. M.; Middleton, C. T.; Luther, B. M.; Zanni, M. T.; Hamm, P.; Krummel, A. T. Breaking Barriers in Ultrafast Spectroscopy and Imaging Using 100 kHz Amplified Yb-Laser Systems. *Acc. Chem. Res.* **2023**, *56* (15), 2062–2071. https://doi.org/10.1021/acs.accounts.3c00152.

(29) Boxer, S. G. Stark Realities. *J. Phys. Chem. B* **2009**, *113* (10), 2972–2983. https://doi.org/10.1021/jp8067393.

(30) Andrews, S. S.; Boxer, S. G. Vibrational Stark Effects of Nitriles I. Methods and Experimental Results. *J. Phys. Chem. A* **2000**, *104* (51), 11853–11863. https://doi.org/10.1021/jp002242r.
(31) Andrews, S. S.; Boxer, S. G. Vibrational Stark Effects of Nitriles II. Physical Origins of Stark Effects from Experiment and Perturbation Models. *J. Phys. Chem. A* **2002**, *106* (3), 469–477. https://doi.org/10.1021/jp011724f.
(32) Silverman, L. N.; Pitzer, M. E.; Ankomah, P. O.; Boxer, S. G.; Fenlon, E. E. Vibrational Stark Effect Probes for Nucleic Acids. *J. Phys. Chem. B* **2007**, *111* (40), 11611–11613. https://doi.org/10.1021/jp0750912.
(33) Suydam, I. T.; Snow, C. D.; Pande, V. S.; Boxer, S. G. Electric Fields at the Active Site of an Enzyme: Direct Comparison of Experiment with Theory. *Science* **2006**, *313* (5784), 200–204. https://doi.org/10.1126/science.1127159.
(34) Weaver, J. B.; Kozuch, J.; Kirsh, J. M.; Boxer, S. G. Nitrile Infrared Intensities Characterize Electric Fields and Hydrogen Bonding in Protic, Aprotic, and Protein Environments. *J. Am. Chem. Soc.* **2022**, *144* (17), 7562–7567. https://doi.org/10.1021/jacs.2c00675.
(35) Edington, S. C.; Flanagan, J. C.; Baiz, C. R. An Empirical IR Frequency Map for Ester C═O Stretching Vibrations. *J. Phys. Chem. A* **2016**, *120* (22), 3888–3896. https://doi.org/10.1021/acs.jpca.6b02887.
(36) Choi, J.-H.; Oh, K.-I.; Lee, H.; Lee, C.; Cho, M. Nitrile and Thiocyanate IR Probes: Quantum Chemistry Calculation Studies and Multivariate Least-Square Fitting Analysis. *J. Chem. Phys.* **2008**, *128* (13), 134506. https://doi.org/10.1063/1.2844787.
(37) Choi, J. H.; Oh, K. I.; Cho, M. Azido-Derivatized Compounds as IR Probes of Local Electrostatic Environment: Theoretical Studies. *J. Chem. Phys.* **2008**, *129* (17), 124503. https://doi.org/10.1063/1.3001915.
(38) Lee, H.; Choi, J.-H.; Cho, M. Vibrational Solvatochromism and Electrochromism. II. Multipole Analysis. *J. Chem. Phys.* **2012**, *137* (11), 114307. https://doi.org/10.1063/1.4751477.
(39) Oh, K.-I.; Lee, J.-H.; Joo, C.; Han, H.; Cho, M. β-Azidoalanine as an IR Probe: Application to Amyloid Aβ(16-22) Aggregation. *J. Phys. Chem. B* **2008**, *112* (33), 10352–10357. https://doi.org/10.1021/jp801558k.
(40) Taskent-Sezgin, H.; Chung, J.; Banerjee, P. S.; Nagarajan, S.; Dyer, R. B.; Carrico, I.; Raleigh, D. P. Azidohomoalanine: A Conformationally Sensitive IR Probe of Protein Folding Protein Structure and Electrostatics. *Angew. Chem. - Int. Ed.* **2010**, *49* (41), 7473–7475. https://doi.org/10.1002/anie.201003325.
(41) Maienschein-Cline, M. G.; Londergan, C. H. The CN Stretching Band of Aliphatic Thiocyanate Is Sensitive to Solvent Dynamics and Specific Solvation. *J. Phys. Chem. A* **2007**, *111* (40), 10020–10025. https://doi.org/10.1021/jp0761158.
(42) Wilderen, L. J. G. W. van; Kern-Michler, D.; M. Müller-Werkmeister, H.; Bredenbeck, J. Vibrational Dynamics and Solvatochromism of the Label SCN in Various Solvents and Hemoglobin by Time Dependent IR and 2D-IR Spectroscopy. *Phys. Chem. Chem. Phys.* **2014**, *16* (36), 19643–19653. https://doi.org/10.1039/C4CP01498G.
(43) Choi, J. H.; Raleigh, D.; Cho, M. Azido Homoalanine Is a Useful Infrared Probe for Monitoring Local Electrostatistics and Sidechain Solvation in Proteins. *J. Phys. Chem. Lett.* **2011**, *2* (17), 2158. https://doi.org/10.1021/JZ200980G.
(44) Błasiak, B.; Lee, H.; Cho, M. Vibrational Solvatochromism: Towards Systematic Approach to Modeling Solvation Phenomena. *J. Chem. Phys.* **2013**, *139* (4), 044111. https://doi.org/10.1063/1.4816041.
(45) Błasiak, B.; Cho, M. Vibrational Solvatochromism. II. A First-Principle Theory of Solvation-Induced Vibrational Frequency Shift Based on Effective Fragment Potential Method. *J. Chem. Phys.* **2014**, *140* (16), 164107. https://doi.org/10.1063/1.4872040.
(46) Błasiak, B.; Cho, M. Vibrational Solvatochromism. III. Rigorous Treatment of the Dispersion Interaction Contribution. *J. Chem. Phys.* **2015**, *143* (16), 164111. https://doi.org/10.1063/1.4934667.
(47) Al-Mualem, Z. A.; Chen, X.; Shirley, J. C.; Xu, C.; Baiz, C. R. BoxCARS 2D IR Spectroscopy with Pulse Shaping. *Opt. Express* **2023**, *31* (2), 2700–2709. https://doi.org/10.1364/OE.471984.
(48) Edington, S. C.; Gonzalez, A.; Middendorf, T. R.; Halling, D. B.; Aldrich, R. W.; Baiz, C. R. Coordination to Lanthanide Ions Distorts Binding Site Conformation in Calmodulin. *Proc. Natl. Acad. Sci.* **2018**, *115* (14), E3126–E3134. https://doi.org/10.1073/pnas.1722042115.
(49) Zhao, R.; Shirley, J. C.; Lee, E.; Grofe, A.; Li, H.; Baiz, C. R.; Gao, J. Origin of Thiocyanate Spectral Shifts in Water and Organic Solvents. *J. Chem. Phys.* **2022**, *156* (10), 104106. https://doi.org/10.1063/5.0082969.
(50) Oh, K.-I.; Choi, J.-H.; Lee, J.-H.; Han, J.-B.; Lee, H.; Cho, M. Nitrile and Thiocyanate IR Probes: Molecular Dynamics Simulation Studies. *J. Chem. Phys.* **2008**, *128* (15), 154504. https://doi.org/10.1063/1.2904558.
(51) Ghosh, D.; Sakpal, S. S.; Chatterjee, S.; Deshmukh, S. H.; Kwon, H.; Kim, Y. S.; Bagchi, S. Association–Dissociation Dynamics of Ionic Electrolytes in Low Dielectric Medium. *J. Phys. Chem. B* **2022**, *126* (1), 239–248. https://doi.org/10.1021/acs.jpcb.1c08613.
(52) Kamlet, M. J.; Abboud, J. L. M.; Abraham, M. H.; Taft, R. W. Linear Solvation Energy Relationships. 23. A Comprehensive Collection of the Solvatochromic Parameters, .Pi.*, .Alpha., and .Beta., and Some Methods for Simplifying the Generalized Solvatochromic Equation. *J. Org. Chem.* **1983**, *48* (17), 2877–2887. https://doi.org/10.1021/jo00165a018.
(53) Zhang, W.; N. Markiewicz, B.; S. Doerksen, R.; Amos B. Smith, I. I. I.; Gai, F. C≡N Stretching Vibration of 5-Cyanotryptophan as an Infrared Probe of Protein Local Environment: What Determines Its Frequency? *Phys. Chem. Chem. Phys.* **2016**, *18* (10), 7027–7034. https://doi.org/10.1039/C5CP04413H.
(54) Marcus, Y. The Properties of Organic Liquids That Are Relevant to Their Use as Solvating Solvents. *Chem. Soc. Rev.* **1993**, *22* (6), 409. https://doi.org/10.1039/cs9932200409.
(55) Shirley, J. C.; Al-Mualem, Z. A.; Baiz, C. R. MeSCN FTIR/2D IR/NLS Data. https://doi.org/10.18738/T8/JLUVIR.
(56) Yuan, R.; Yan, C.; Fayer, M. Ion–Molecule Complex Dissociation and Formation Dynamics in LiCl Aqueous Solutions from 2D IR Spectroscopy. *J. Phys. Chem. B* **2018**, *122* (46), 10582–10592. https://doi.org/10.1021/acs.jpcb.8b08743.
(57) Yuan, R.; Fayer, M. D. Dynamics of Water Molecules and Ions in Concentrated Lithium Chloride Solutions Probed with Ultrafast 2D IR Spectroscopy. *J. Phys. Chem. B* **2019**, *123* (35), 7628–7639. https://doi.org/10.1021/acs.jpcb.9b06038.
(58) Asbury, J. B.; Steinel, T.; Kwak, K.; Corcelli, S. A.; Lawrence, C. P.; Skinner, J. L.; Fayer, M. D. Dynamics of Water Probed with Vibrational Echo Correlation Spectroscopy. *J. Chem. Phys.* **2004**, *121* (24), 12431–12446. https://doi.org/10.1063/1.1818107.

(59) Kwak, K.; Park, S.; Fayer, M. D. Dynamics around Solutes and Solute–Solvent Complexes in Mixed Solvents. *Proc. Natl. Acad. Sci.* **2007**, *104* (36), 14221–14226. https://doi.org/10.1073/pnas.0701710104.
(60) King, J. T.; Baiz, C. R.; Kubarych, K. J. Solvent-Dependent Spectral Diffusion in a Hydrogen Bonded "Vibrational Aggregate." *J. Phys. Chem. A* **2010**, *114* (39), 10590–10604. https://doi.org/10.1021/jp106142u.
(61) Baiz, C. R.; Kubarych, K. J.; Geva, E.; Sibert, E. L. Local-Mode Approach to Modeling Multidimensional Infrared Spectra of Metal Carbonyls. *J. Phys. Chem. A* **2011**, *115* (21), 5354–5363. https://doi.org/10.1021/jp201641h.
(62) Li, S.; Schmidt, J. R.; Corcelli, S. A.; Lawrence, C. P.; Skinner, J. L. Approaches for the Calculation of Vibrational Frequencies in Liquids: Comparison to Benchmarks for Azide/Water Clusters. *J. Chem. Phys.* **2006**, *124* (20), 204110. https://doi.org/10.1063/1.2200690.
(63) Li, S.; Schmidt, J. R.; Piryatinski, A.; Lawrence, C. P.; Skinner, J. L. Vibrational Spectral Diffusion of Azide in Water. *J. Phys. Chem. B* **2006**, *110* (38), 18933–18938. https://doi.org/10.1021/jp057568k.
(64) Li, S.; Schmidt, J. R.; Skinner, J. L. Vibrational Energy Relaxation of Azide in Water. *J. Chem. Phys.* **2006**, *125* (24), 244507. https://doi.org/10.1063/1.2408421.
(65) Lindquist, B. A.; Haws, R. T.; Corcelli, S. A. Optimized Quantum Mechanics/Molecular Mechanics Strategies for Nitrile Vibrational Probes: Acetonitrile and Para-Tolunitrile in Water and Tetrahydrofuran. *J. Phys. Chem. B* **2008**, *112* (44), 13991–14001. https://doi.org/10.1021/jp804900u.
(66) Lindquist, B. A.; Corcelli, S. A. Nitrile Groups as Vibrational Probes: Calculations of the C≡N Infrared Absorption Line Shape of Acetonitrile in Water and Tetrahydrofuran. *J. Phys. Chem. B* **2008**, *112* (20), 6301–6303. https://doi.org/10.1021/jp802039e.
(67) Layfield, J. P.; Hammes-Schiffer, S. Calculation of Vibrational Shifts of Nitrile Probes in the Active Site of Ketosteroid Isomerase upon Ligand Binding. *J. Am. Chem. Soc.* **2013**, *135* (2), 717–725. https://doi.org/10.1021/ja3084384.
(68) Liu, C. T.; Layfield, J. P.; Stewart, R. J. I.; French, J. B.; Hanoian, P.; Asbury, J. B.; Hammes-Schiffer, S.; Benkovic, S. J. Probing the Electrostatics of Active Site Microenvironments along the Catalytic Cycle for Escherichia Coli Dihydrofolate Reductase. *J. Am. Chem. Soc.* **2014**, *136* (29), 10349–10360. https://doi.org/10.1021/ja5038947.
(69) Brünig, F. N.; Geburtig, O.; Canal, A. von; Kappler, J.; Netz, R. R. Time-Dependent Friction Effects on Vibrational Infrared Frequencies and Line Shapes of Liquid Water. *J. Phys. Chem. B* **2022**, *126* (7), 1579–1589. https://doi.org/10.1021/acs.jpcb.1c09481.